RSC Advances

PAPER

View Article Online
View Journal | View Issue

Cite this: *RSC Adv.*, 2022, **12**, 420

Luminescence properties, energy transfer and thermal stability of white emitting phosphor $Sr_3(PO_4)_2$:Ce^{3+}/Tb^{3+}/Mn^{2+} for white LEDs

Yingshan Ma,[a] Suyue Fu,[a] Yichang Zhao,[a] Chunjiao Liu,*[a] Leipeng Li,[a] Zhijun Wang,*[a] Hao Suo,[a] Dawei Wang,[b] Jinxin Zhao[b] and Panlai Li*[a]

Received 3rd November 2021
Accepted 15th December 2021

DOI: 10.1039/d1ra08062h

rsc.li/rsc-advances

A series of $Sr_3(PO_4)_2$:Ce^{3+}/Mn^{2+}/Tb^{3+} phosphors were synthesized by a high temperature solid phase method. After introducing Ce^{3+} as sensitizer in $Sr_3(PO_4)_2$:Ce^{3+}/Mn^{2+}, the efficient energy transfer from Ce^{3+} to Mn^{2+} was observed and analyzed in detail, and $Sr_3(PO_4)_2$:Ce^{3+}/Mn^{2+} was demonstrated to be color tunable, changing from blue to orange red. In addition, Tb^{3+} ion, which mainly emits green light, was further added into the $Sr_3(PO_4)_2$:Ce^{3+}/Mn^{2+}. Due to the addition of this green emission, the white emitting phosphors with good quality were obtained. At the same time, the energy transfer mechanisms among Ce^{3+}, Tb^{3+} and Mn^{2+} ions were also analyzed in detail. The results show that $Sr_3(PO_4)_2$:Ce^{3+}/Mn^{2+}/Tb^{3+} is a promising candidate for white light emitting diodes.

1 Introduction

In recent years, solid-state light sources have been widely used because of their advantages such as long lifetime, high emitting intensity, excellent conversion efficiency and environmental friendliness. In order to better meet the demand of applications, it is essential to obtain phosphors with adjustable emission bands.[1–5] Typically, the tuning-color can be achieved *via* energy transfer from sensitizer to activator, such as Ce^{3+}–Tb^{3+}, Ce^{3+}–Mn^{2+}, Tb^{3+}–Mn^{2+} or Eu^{2+}–Mn^{2+}.[6–10] Through matrix component regulation and cation substitution, the crystal field environment surrounding the luminescent centers can be changed, thus causing the tunable luminescence phenomenon.[11–13] Phosphate has been widely studied in the field of optics because of its stable structure and excellent chemical properties.[14,15] $Sr_3(PO_4)_2$ (SPO) is a common and classical phosphate, which, however, has been less studied in the field of luminescent materials over past decades. In addition, only several kinds of activators have been briefly studied in the host of SPO. Therefore, it is necessary to investigate the luminescence features of typical luminescent centers in SPO. In this work, a series of Ce^{3+}, Tb^{3+} and Mn^{2+} singly- or codoped SPO were synthesized, and the energy transfer can be observed from the codoped phosphors. The results show that these phosphors may be application in the white lighting diodes.

2 Sample preparation and characterization

2.1 Sample preparation

A series of SPO:$x$$Ce^{3+}$, SPO:$x$$Ce^{3+}$, $z$$Mn^{2+}$ and SPO:0.08Ce^{3+}, $y$$Tb^{3+}$, 0.05$Mn^{2+}$ were synthesized by the high temperature solid state method. The raw materials were $SrCO_3$ (99.99%), $MnCO_3$ (99.99%), Eu_2O_3 (99.99%), CeO_2 (99.99%), $NH_4H_2PO_4$ (99.99%) and Tb_4O_7 (99.99%). Firstly, the raw materials, according to the calculated chemical formula, were weighed and fully grinded by an agate mortar by 20 minutes to form uniform powder. Next, the mixture was loaded into corundum crucible and calcined at 960 °C for 300 min in air to achieve the final samples in the box-type furnace.

2.2 Characterization

The structure of sample was characterized by German Bruker D8 Xray diffractometer (Cu target Kα, $\lambda = 0.15406$ nm). The voltage and current are 40 kV and 40 mA, respectively. The scan range of 2θ degree and step size are 10–80° and 0.02°, respectively. The spectra of samples were measured by Horiba FL-4600 fluorescence spectrometer. The fluorescence lifetime of samples was measured by Horiba FL-1057 fluorescence spectrometer, and the excitation sources are nano-LED emitting at 335 nm and Xe lamp. The steady state transient fluorescence spectrometer of Horibafl-4600 was used to measure the fluorescence attenuation curve of the sample.

3 Results and discussion

3.1 Crystal structure

Fig. 1(a–c) show the XRD patterns of SPO:Ce^{3+}, SPO:Ce^{3+}, Mn^{2+} and SPO:0.08Ce^{3+}, Tb^{3+}, 0.05Mn^{2+}, respectively. It can be seen

[a]National-Local Joint Engineering Laboratory of New Energy Photoelectric Devices, Hebei Key Laboratory of Optic-electronic Information and Materials, College of Physics Science & Technology, Hebei University, Baoding 071002, China. E-mail: 1342687874@qq.com; wangzj1998@126.com; li_panlai@126.com

[b]Hebei Key Laboratory of Semiconductor Lighting and Display Critical Materials, Baoding, 071000, China

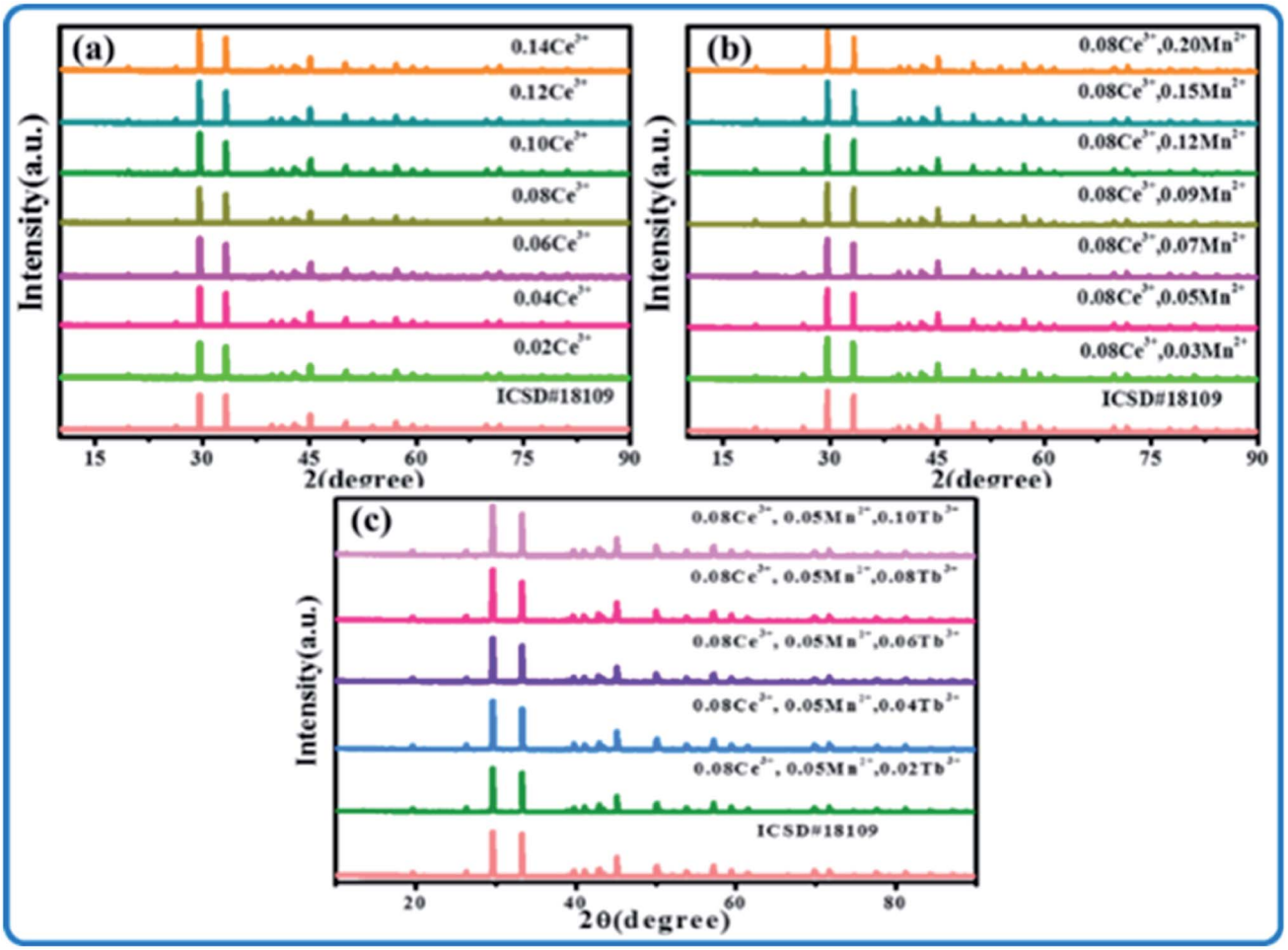

Fig. 1 XRD patterns of (a) SPO:xCe^{3+}, (b) SPO:0.08Ce^{3+}, zMn^{2+}, and (c) SPO:0.08Ce^{3+}, yTb^{3+}, 0.05Mn^{2+}.

that no redundancy diffraction peaks appeared for all samples, indicating that the as-synthesized samples are all of single crystal phase. The introduction of luminescent centers Ce^{3+}, Tb^{3+} and Mn^{2+} has no influence on the crystal structure of SPO. In order to further inspect the minor change of SPO induced by Ce^{3+}, Tb^{3+} and Mn^{2+}, Rietveld refinement was performed on all samples, and the results are shown in Fig. 2, Tables 1 and 2. The parameters of R_p, R_{wp} and χ^2 are all within the range of reliable values. According to the refined data presented in Table 1, as Ce^{3+} ions gradually entered into SPO, the volume V gradually increased. As is well known, if an ion with smaller radius enters into lattice site, the lattice volume is expected to shrink. However, as the number of Ce^{3+}($r = 0.108$ Å, $N = 6$; $r = 0.125$ Å, $N = 10$)ions gradually increased, the volume V gradually increased. The reason for this phenomenon is as follows there are some Ce^{3+} ions in the gap of lattice, which makes the volume V increase gradually.[16,17]

3.2 Luminescence characteristics of $Sr_3(PO_4)_2$:Ce^{3+}

Fig. 3(a and b) display the emission and excitation spectra of SPO:xCe^{3+}, respectively. The excitation band ranges from 240 to 320 nm with center wavelength at 292 nm. And the emission band is also a broad spectrum, which is located in the range of 300–450 nm and peaked at 348 nm. The optimal concentration of Ce^{3+} is 8% in molar ratio. In addition, it can be found that the emission band of Ce^{3+} is asymmetrical, which is composed of two sub-lines with peak at 338 and 359 nm, respectively (Fig. 4(a)). In order to determine the origin of these two sub-peaks, their decay curves were measured, as shown in Fig. 4(b). The 338 and 359 nm emission bands' lifetimes were fitted to be 13.02 and 22.65 ns, respectively, which reveals that these two emission bands came from two different lattice site, Sr_1 and Sr_2 in the matrix SPO.[18,19]

According to the above analysis, the transition process of Ce^{3+} is shown in Fig. 5(a). Fig. 5(b) presents the normalized emission spectra of SPO embedded with different concentration of Ce^{3+}. With the gradual increment of Ce^{3+} into SPO, there is a red-shift of ~7 nm for the emission band, which is likely to stem from the change of crystal field around Ce^{3+}. As depicted in Fig. 5(a), the change of crystal field has effect on the 5d state of Ce^{3+}, thus affecting the energy difference between the excited state and ground state. The larger the splitting of the 5d state, the closer the ground state and excited state. The cleavage of state is related to the charge of crystal field around central ion, and the cleavage becomes stronger when the charge of central

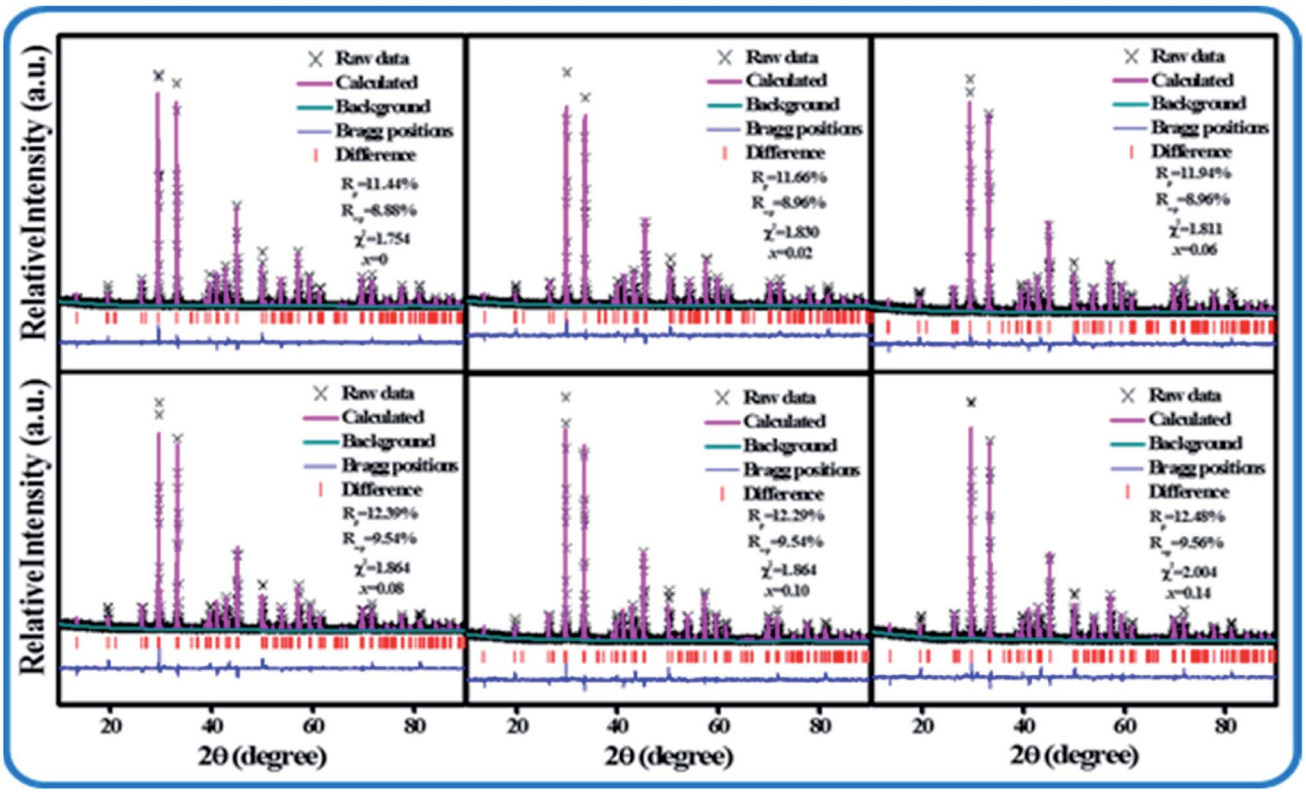

Fig. 2 XRD refinement of SPO:xCe^{3+}.

Table 1 Rietveld refinement results SPO:xCe^{3+}

SPO:xCe^3	$a = b = c$	V	R_p	R_{wp}	χ^2
$x = 0$	7.2923	165.834	8.88%	11.44%	1.754
$x = 0.02$	7.2929	166.842	8.96%	11.66%	1.830
$x = 0.06$	7.2947	166.843	9.08%	11.94%	1.794
$x = 0.08$	7.2942	166.869	9.56%	12.39%	1.967
$x = 0.10$	7.2949	166.882	9.54%	12.29%	1.864
$x = 0.14$	7.2958	165.899	9.56%	12.48%	2.004

Table 2 Bond length and twist degree of SPO:xCe^{3+}

SPO:xCe^{3+}	0	0.02	0.06	0.08	0.10	0.14
Sr_1–O_2	2.62392	2.62407	2.62431	2.62433	2.62456	2.62458
Sr_2–O_1	2.47392	2.47397	2.47416	2.47429	2.47440	2.47445
Sr_2–O_2	2.63424	2.63440	2.63464	2.63466	2.63489	2.63492
Sr_2–O_2	2.72923	2.72916	2.72913	2.72902	2.72885	2.72855
Distortion	0.06483	0.06478	0.06456	0.06447	0.06442	0.06439

ion is larger. In our work, with the increase of the doping concentration of Ce^{3+} ions, the distance of the luminescence center is shortened, and the non-radiative transition is enhanced. The loss of part of the energy leads to the shift of the spectrum to the long wave and the redshift of the spectrum.

3.3 Luminescence characteristics of $Sr_3(PO_4)_2$:0.08Ce^{3+}, zMn^{2+}

The emission spectra and excitation spectra of SPO:0.08Ce^{3+}, zMn^{2+} are shown in Fig. 6. Upon the excitation at 292 nm, there are two main emission bands peaking at 380 and 616 nm that are ascribed to the emissions from Ce^{3+} and Mn^{2+}. It can also be seen from the emission spectra that with the gradual increase of Ce^{3+}, the emitting intensity of Mn^{2+} had been greatly improved. As clearly presented in Fig. 7(a), there is an overlap between the emission spectra of Ce^{3+} and the excitation spectra of Mn^{2+}, suggesting a possible energy transfer from Ce^{3+} to Mn^{2+}. With the gradual increase of Mn^{2+}, the emission intensity of Ce^{3+} showed downtrend. These results indicate that the energy transfer from Ce^{3+} to Mn^{2+} exists in SPO.

To further inspect this mechanism, we calculated the critical distance Rc between two types of ions according to the following formula[20]

$$R_C = 2\left[\frac{3V}{4\pi X_C N}\right]^{1/3} \quad (1)$$

where N represents the number of cations in crystal lattice, X_c is the concentration of doped ions, and V represents the volume of crystal lattice. For SPO, N and V are 3 and 494.73 Å, respectively. The doping concentration of Mn^{2+} was set to be the maximum doping concentration of $X_c = 0.20$. The critical distance R_c between Ce^{3+} ions and Mn^{2+} was calculated to be 11.64 Å. It is known that there are several kinds of mechanisms, including exchange interaction, multipolar interaction and radiation

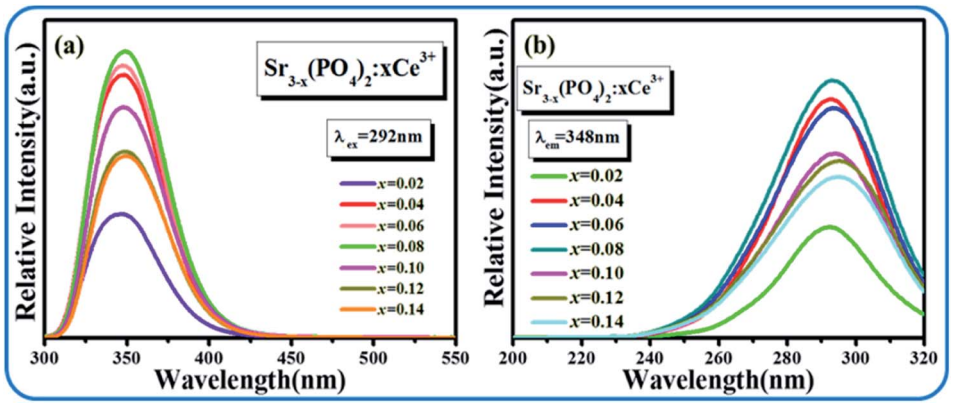

Fig. 3 Emission spectra and excitation spectra of SPO:xCe^{3+}.

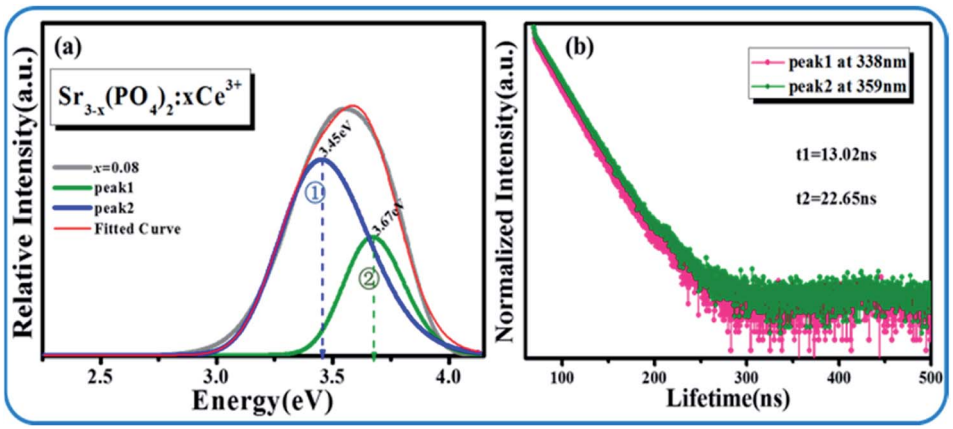

Fig. 4 (a) Gaussian fitting emission peaks of SPO:Ce^{3+}; (b) SPO:Energy level diagram of Ce^{3+}.

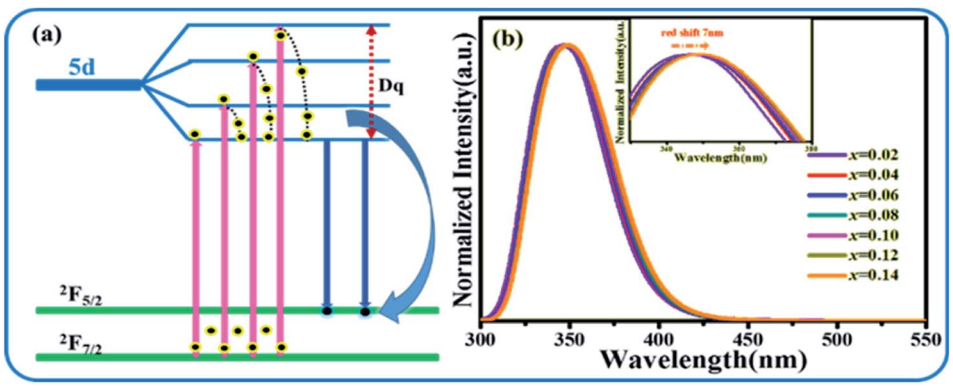

Fig. 5 (a) Energy diagram that shows the splitting condition of 5d state. (b) Emission spectra of SPO:xCe^{3+}.

reabsorption. Only when the critical distance R_c is less than 5 Å, the exchange interaction may occur. Moreover, the radiation reabsorption could also be excluded. Therefore, the energy transfer between Ce^{3+} and Mn^{2+} in SPO is the multipolar interaction.

In order to more accurately determine the energy transfer between Ce^{3+} and Mn^{2+}, the fluorescence decay curves of the 380 nm emission line were monitored, as shown in Fig. 8, and the calculated lifetimes were also listed in this figure. All the curves can be well fitted to a second-exponential function as follows[21]

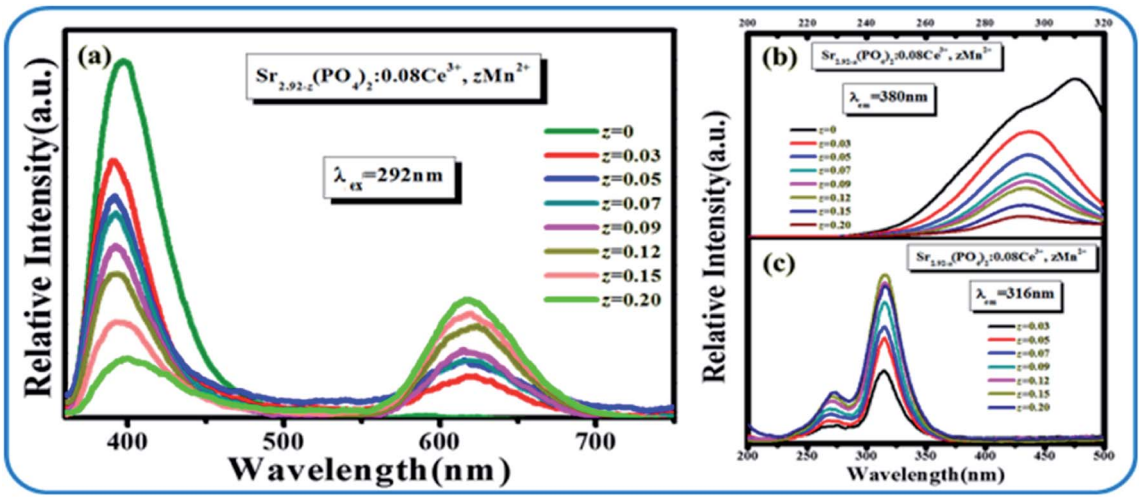

Fig. 6 (a) Emission spectra of SPO:0.08Ce^{3+}, zMn^{2+}. Excitation spectra SPO:0.08Ce^{3+}, zMn^{2+} monitored at (b) 380 nm and at (c) 616 nm, respectively.

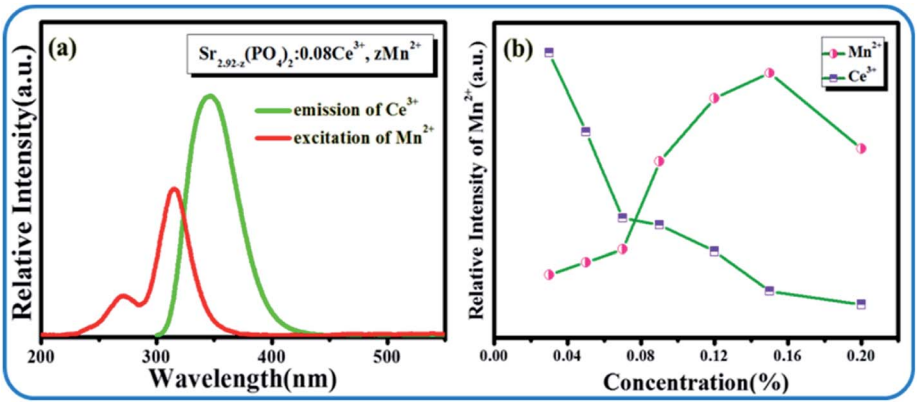

Fig. 7 (a) Excitation spectra of Mn^{2+} (red line) and emission spectra of Ce^{3+} (green line); (b) emission intensity of Mn^{2+} and Ce^{3+} with different Mn^{2+} concentrations.

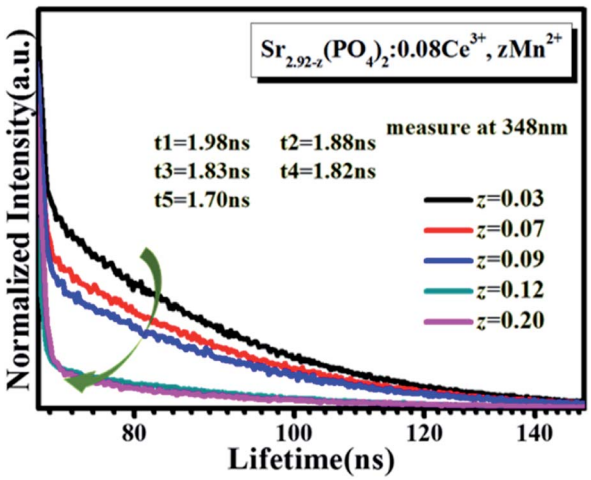

Fig. 8 Decay curves of SPO:0.08Ce^{3+}, zMn^{2+}.

$$I(t) = A_1 \exp\left(-\frac{t}{\tau_1}\right) + A_2 \exp\left(-\frac{t}{\tau_2}\right) \quad (2)$$

Where $I(t)$ is the luminescence intensity, A_1 and A_2 are fitting consiants, t is the time, and τ_1 and τ_2 are the lifetimes of the exponential component. It can be seen from Fig. 8 that the lifetime of Ce^{3+} decreased gradually with the gradual increase of doping concentration of Mn^{2+}. It confirms the presence of energy transfer from Ce^{3+} to Mn^{2+}, and the specific processes are shown in Fig. 9. Upon excitation at 292 nm, the Ce^{3+} ions jump from 4f to 5d state and then to the final emitting state, followed by the generation of emission. Meanwhile, because the energy level of Mn^{2+} is lower than that of Ce^{3+}, some Ce^{3+} ions will transition from 5d state to the 3d state of Mn^{2+}, leading to the luminescence of Mn^{2+}. Fig. 10 shows the relationship between I_{s0}/I_s and $c^{\alpha/3}$, and α was fitted to be 6. It indicates that the energy transfer between Ce^{3+} and Mn^{2+} in SPO belongs to the dipole–dipole interaction.

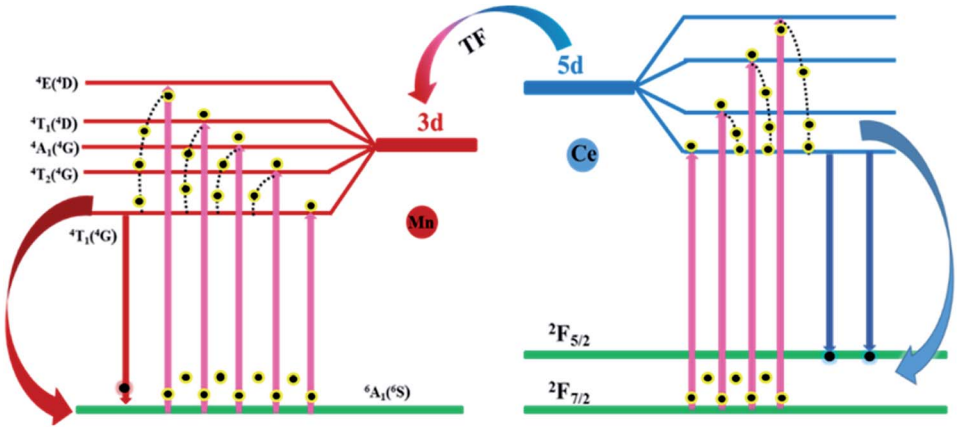

Fig. 9 Energy transfer mechanism diagram of SPO:0.08Ce^{3+}, zMn^{2+}.

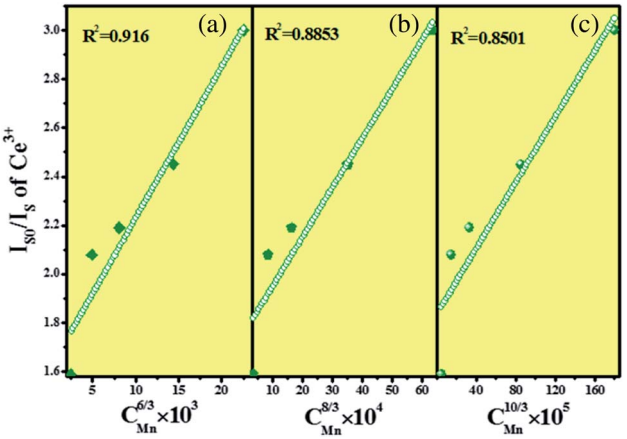

Fig. 10 Dependence of I_{s0}/I_s on (a) $C^{6/3}$, (b) $C^{8/3}$, (c) $C^{10/3}$.

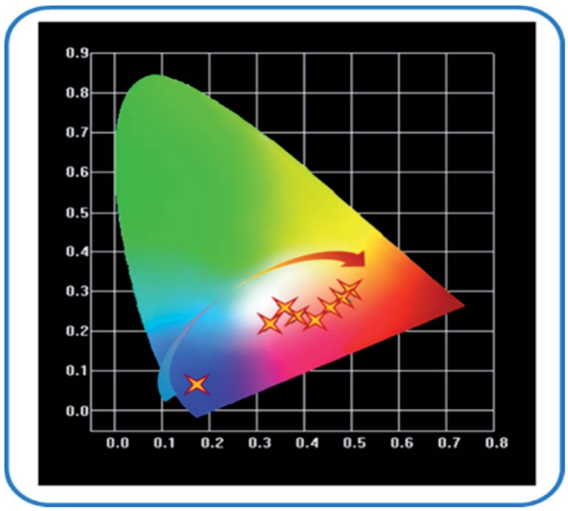

Fig. 11 SPO:0.08Ce^{3+}, zMn^{2+} color coordinate changes.

According to the emission spectra of samples, the color coordinate diagram of SPO:0.08Ce^{3+}, zMn^{2+} was obtained, as shown in Fig. 11. It can be seen from this CIE diagram that with the rise of doping concentration of Mn^{2+}, the emission color of SPO:0.08Ce^{3+}, zMn^{2+} moves from blue to orange-red. It reveals that Ce^{3+} has a significant effect on the luminescence of Mn^{2+}. Therefore, a series of phosphors with variable colors can be obtained.

3.4 Analysis of luminescence characteristics of $Sr_3(PO_4)_2$:0.08Ce^{3+}, yTb^{3+} and 0.05Mn^{2+}

Although the emission color of SPO:0.08Ce^{3+}, zMn^{2+} can be tuned from blue to orange-red, this phosphor lacks green light, which hinders the production of white emission. To solve this problem, Tb^{3+} ion, which is known to be a typical luminescent center for green light, is introduced into the phosphor of SPO:Ce^{3+}, Mn^{2+}, of which the emission spectra are presented in Fig. 12(a). Fig. 12(b–d) shows the emission intensity of Ce^{3+}, Tb^{3+} and Mn^{2+} as a function of doping concentration. With the increase of Tb^{3+}, the emission intensity of Ce^{3+} decreased, while that of Tb^{3+} and Mn^{2+} gradually increased. Fig. 13(a–c) represent the excitation spectra of Ce^{3+}, Tb^{3+}, and Mn^{2+}, and Fig. 14 presents the affiliations corresponding to the emission peak of SPO:0.08Ce^{3+}, yTb^{3+}, 0.05Mn^{2+}. The 380 nm emission line corresponds to the 5d → $^2F_{5/2}$/$^2F_{7/2}$ transition of Ce^{3+}. The emission bands at 420, 440, 500, 550 and 598 nm are ascribed to the $^5D_3 \rightarrow {}^7F_5$, $^5D_3 \rightarrow {}^7F_4$, $^5D_4 \rightarrow {}^7F_6$, $^5D_4 \rightarrow {}^7F_5$ and $^5D_4 \rightarrow {}^7F_4$ transitions of Tb^{3+}, respectively. The 625 nm emission line comes from the $^4T_1(^4G)$–$^6A_1(^6S)$ transition. From the emission spectra, it can be seen that the Ce^{3+} emission decreased while the emission intensity of Tb^{3+} and Mn^{2+} increased, which is likely attributed to the energy transfer from Ce^{3+} to Tb^{3+} and Mn^{2+}. The fluorescence decay curves of Ce^{3+} and Tb^{3+} ions in SPO:0.08Ce^{3+}, yTb^{3+} and SPO:0.08Ce^{3+}, yTb^{3+}, 0.05Mn^{2+} were measured, as shown in Fig. 15(a–d). And the calculated lifetimes are depicted in Fig. 16(a and b). From the emission spectra, it can be seen that the decrease rate of Ce2 is higher than that of

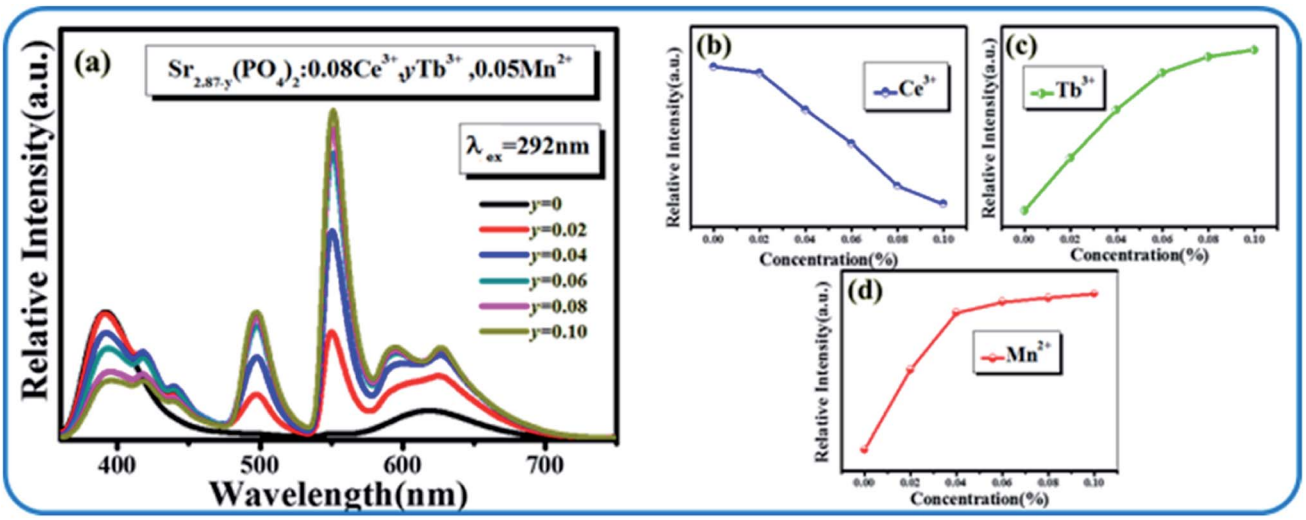

Fig. 12 (a) Emission spectra of SPO:0.08Ce^{3+}, yTb^{3+} and 0.05Mn^{2+}; Emission intensities of Ce^{3+} (b), Tb^{3+} (c) and Mn^{2+}, respectively (d).

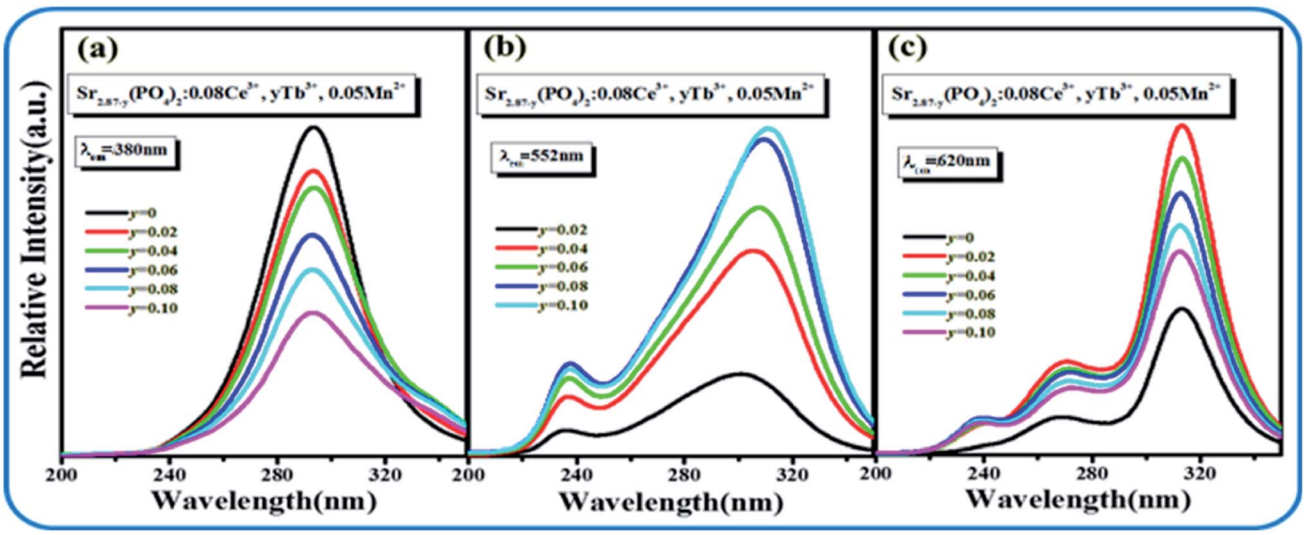

Fig. 13 Excitation spectra of Ce^{3+} (a), Tb^{3+} (b) and Mn^{2+} (c), respectively.

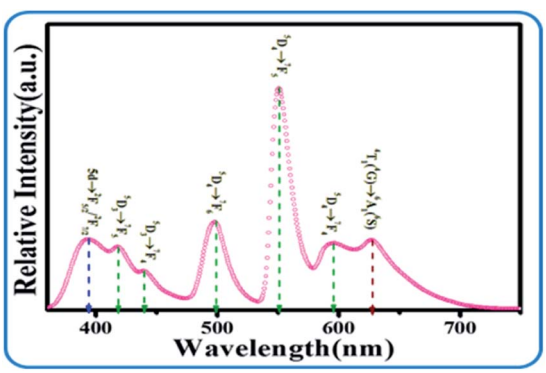

Fig. 14 Energy level transition diagram of SPO:0.08Ce^{3+} and yTb^{3+}, 0.05Mn^{2+}.

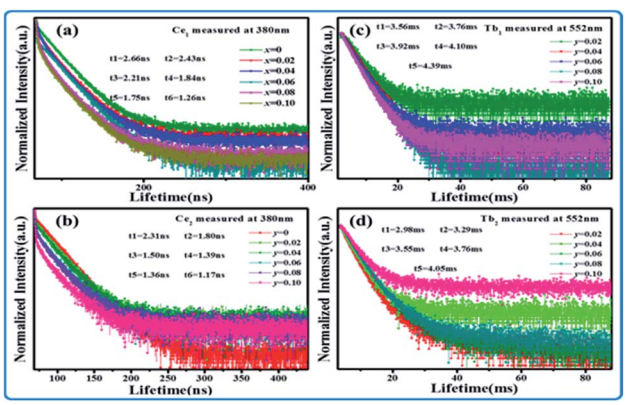

Fig. 15 Decay curve of (a) Ce_1, (b) Ce_2, (c) Tb_1 and (d) Tb_2.

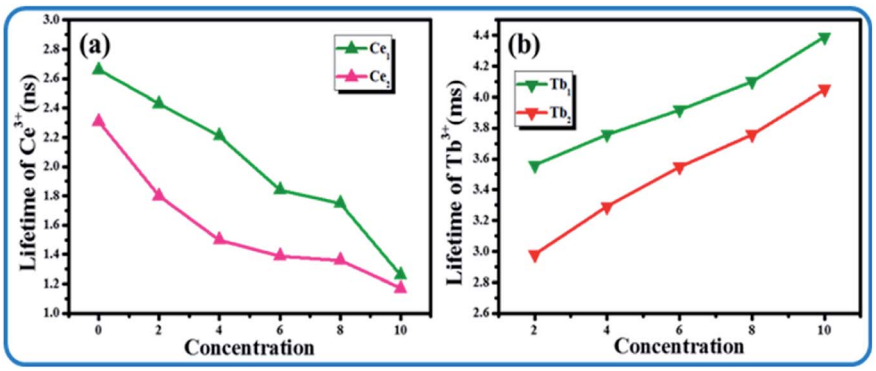

Fig. 16 Lifetime of (a) Ce^{3+} and (b) Tb^{3+} as a function of doping concentration.

Table 3 Color rendering index, color coordinates and color temperature of SPO:0.08Ce^{3+}, $y$$Tb^{3+}$, 0.05$Mn^{2+}$

SPO:0.08Ce^{3+}, $y$$Tb^{3+}$, 0.05$Mn^{2+}$	CRI	(X, Y)	CCT (K)
$y = 0$	6.3	(0.373, 0.217)	3743
$y = 0.02$	45.5	(0.376, 0.337)	3777
$y = 0.04$	59.3	(0.380, 0.391)	4115
$y = 0.06$	62.6	(0.376, 0.426)	4394
$y = 0.08$	59.4	(0.382, 0.446)	4367
$y = 0.10$	57.8	(0.383, 0.455)	4373

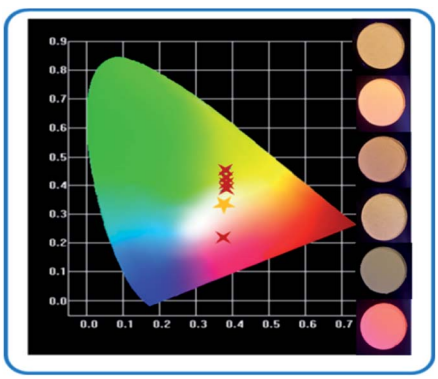

Fig. 17 Color coordinates of SPO:0.08Ce^{3+}, $y$$Tb^{3+}$, 0.05$Mn^{2+}$.

Ce1, while the change rate of the lifetime of Tb^{3+} is almost a constant, confirming that the increase of Mn^{2+} emission is due to the energy transfer from Ce^{3+}.

It can be seen that the main emission peak of SPO:0.08Ce^{3+}, $y$$Tb^{3+}$, 0.05$Mn^{2+}$ is located at about 550 nm, which perfectly complements the missing green light of the emission spectrum of SPO:0.08Ce^{3+}, $z$$Mn^{2+}$. The color rendering index, color coordinates and dependence on temperature of SPO:0.08Ce^{3+}, $y$$Tb^{3+}$, 0.05$Mn^{2+}$ are given in Table 3. According to this table, the color coordinate of SPO:0.08Ce^{3+}, $y$$Tb^{3+}$, 0.05$Mn^{2+}$ is depicted in Fig. 17. Obviously, the chromaticity coordinate could locate in the white light range *via* a careful adjustment of the doping concentration of Tb^{3+}.

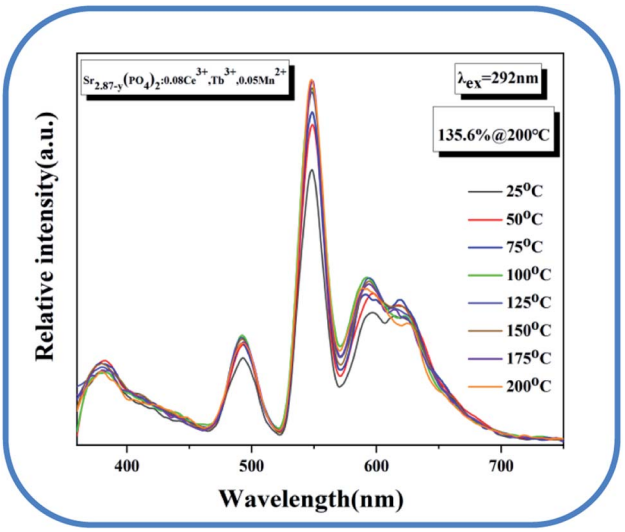

Fig. 18 Temperature spectrum of $Sr_{2.87-y}(PO_4)_2$:0.08Ce^{3+}, Tb^{3+}, 0.05Mn^{2+}.

The temperature spectrum of the sample is shown in Fig. 18. The picture shows that the luminous intensity can still maintain 135.6% of that at room temperature at 200 degrees, showing the good temperature stability of the material.

4 Conclusions

In summary, a series of SPO:$x$$Ce^{3+}$, SPO:$x$$Ce^{3+}$, $z$$Mn^{2+}$ and SPO:0.08Ce^{3+}, $y$$Tb^{3+}$, 0.05$Mn^{2+}$ phosphors were synthesized. For $Sr_3(PO_4)_2$:Ce^{3+}, Mn^{2+}, the efficient energy transfer from Ce^{3+} to Mn^{2+} was observed and analyzed in detail, and the tunable emission color of $Sr_3(PO_4)_2$:Ce^{3+}–Mn^{2+} was realized by the energy transfer. In addition, Tb^{3+} ion, which mainly emits green light, was further added into $Sr_3(PO_4)_2$:Ce^{3+}, Mn^{2+}. Due to the addition of this green emission, the white emitting phosphors with good quality were obtained. At the same time, the energy transfer mechanisms among Ce^{3+}, Tb^{3+} and Mn^{2+} ions were also analyzed in detail. The results show that $Sr_3(PO_4)_2$:Ce^{3+}, Mn^{2+}, Tb^{3+} is a promising candidate for white LEDs.

Conflicts of interest

The authors declare no competing financial interest.

Acknowledgements

The work is supported by the National Natural Science Foundation of China (No. 51902080), the Natural Science Foundation of Hebei Province, China (No. E2019201223), the Personnel Training Project of Hebei Province, China (No. A201902005), and the Central Government to Guide Local Scientific and Technological Development (No. 206Z1102G, 216Z1101G).

References

1 M. Shang, C. Li and J. Lin, How to produce white light in a single-phase host, *Chem. Soc. Rev.*, 2014, **43**(5), 1372–1386.
2 S. Ye, F. Xiao, Y. X. Pan, *et al.*, Phosphors in phosphor-converted white light-emitting diodes: Recent advances in materials, techniques and properties, *Mater. Sci. Eng., R*, 2010, **71**(1), 1–34.
3 C. C. Lin and R. S. Liu, Advances in phosphors for light-emitting diodes, *J. Phys. Chem. Lett.*, 2011, **2**(11), 1268–1277.
4 X. Li, P. Li, Z. Wang, *et al.*, Color-tunable luminescence properties of Bi^{3+} in $Ca_5(BO_3)3F$ via changing site occupation and energy transfer, *Chem. Mater.*, 2017, **29**(20), 8792–8803.
5 M. Chen, Z. Xia, M. S. Molokeev, *et al.*, Tuning of photoluminescence and local structures of substituted cations in $Sr_2Ca(PO_4)_{2-(1-x)}Ca_{10}Li(PO_4)_7$:$Eu^{2+}$ phosphors, *Chem. Mater.*, 2017, **29**(3), 1430–1438.
6 J. Huo, L. Wei, B. Shao, *et al.*, Color tunable emission via efficient $Ce^{3+}\rightarrow Tb^{3+}$ energy transfer pair in $MgYSi_2O_5N$ oxynitride phosphor for near-UV-pumped white LEDs, *Dyes Pigm.*, 2017, **139**, 174–179.
7 D. Yun, L. Liangbo, L. Min, *et al.*, Efficient manganese luminescence induced by Ce^{3+}-Mn^{2+} energy transfer in rare earth fluoride and phosphate nanocrystals, *Nanoscale Res. Lett.*, 2011, **6**(1), 119.
8 Y. Jia, L. Wei, N. Guo, *et al.*, Realization of color hue tuning via efficient Tb^{3+}–Mn^{2+} energy transfer in $Sr_3Tb(PO_4)_3$: Mn^{2+}, a potential near-UV excited phosphor for white LEDs, *Phys. Chem. Chem. Phys.*, 2013, **15**(16), 6057.
9 C. H. Huang, T. M. Chen, W. R. Liu, *et al.*, A Single-Phased Emission-Tunable Phosphor $Ca_9Y(PO_4)_7$: Eu^{2+},Mn^{2+} with Efficient Energy Transfer for White-Light-Emitting Diodes, *ACS Appl. Mater. Interfaces*, 2010, **2**(1), 259–264.
10 P. Chen, *New phenomenon, mechanism and application of rare earth ion fluorescence*. Zhejiang University, 2016. in Chinese.
11 Y. C. Jia, Y. J. Huang, Y. H. Zheng, *et al.*, Color point tuning of $Y_3Al_5O_{12}$:Ce^{3+} phosphor via Mn^{2+}-Si^{4+} incorporation for white light generation, *J. Mater. Chem.*, 2012, **22**(30), 15146–15152.
12 L. Ye, X. Peng, S. Zhang, *et al.*, Photoluminescence properties of Ca-doped $BaMgAl_{10}O_{17}$:Eu^{2+},Mn^{2+} blue phosphor using BaF_2 and CaF_2 as co-flux, *J. Rare Earths*, 2014, **32**(12), 1109–1113.
13 N. Guo, H. You, Y. Song, *et al.*, White-light emission from a single-emitting-component $Ca_9Gd(PO_4)_7$:Eu^{2+},Mn^{2+} phosphor with tunable luminescent properties for near-UV light-emitting diodes, *J. Mater. Chem.*, 2010, **20**(41), 9061–9070.
14 Y. Dongyan, W. Xingya, Y. Gongqin and C. Jieliang, Research Progress of Rare Earth Doped Phosphate Phosphors, *Mater. Rev.*, 2020, **34**, 41–47.
15 Z. Fangyi, C. Hao, S. Zhen and L. Quanlin, Structural Confinement for Cr^{3+} Activators toward Efficient Nearinfrared Phosphors with Suppressed Concentration Quenching, *Chem. Mater.*, 2021, **33**(10), 3621–3630.
16 Y. Wang, J. Ding and Y. Wang, Preparation and photoluminescence properties with the site-selected excitations of Bi^{3+}-activated $Ba_3Sc_4O_9$ phosphors, *J. Am. Ceram. Soc.*, 2017, **100**(6), 2612–2620.
17 R. Cui, X. Guo, X. Gong, *et al.*, Enhancing red emission of $CaBi_2Ta_2O_9$: Eu^{3+} phosphor by La^{3+} co-doping, *J. Mater. Sci.: Mater. Electron.*, 2016, **27**(9), 9656–9660.
18 P. Dorenbos, 5d -level energies of Ce^{3+}, and the crystalline environment.I.Fluoridecompounds, *Phys. Rev. B: Condens. Matter Mater. Phys.*, 2000, **62**(23), 15640–15649.
19 Y. Q. Li, N. Hirosaki, R. J. Xie, *et al.*, ChemInform Abstract: Yellow-Organe-Emitting $CaAlSiN_3$:Ce^{3+} Phosphor: Structure, Photoluminescence, and Application in White LEDs, *ChemInform*, 2008, **20**(21), 6704–6714.
20 G. Blasse, *J. Solid State Chem.*, 1986, **62**, 207–211.
21 Z. Ming, J. Zhao, H. C. Swart and Z. Xia, *J. Rare Earths*, 2020, **38**, 506.